First submitted version. A reviewed and edited version of this paper was published in Environmental Modelling & Software (doi: 10.1016/j.envsoft.2014.10.015)

Evaluation and validation of a nested-grid implementation for 3D finite-difference Cartesian semi-implicit hydrodynamic models in two real applications: Sacramento River and Lake Tahoe

Mario Acosta[(1),(2),(5),*], Mancia Anguita[(1),(5)], F. Javier Fernández-Baldomero[(1)], Cintia L. Ramón[(2),(4)], S. Geoffrey Schladow [(3),(6)] and Francisco J. Rueda[(2),(4)]

(1) Dept. of Computer Architecture, University of Granada, C/ Periodista Daniel Saucedo Aranda s/n, Granada, Spain
(2) Water Research Institute, University of Granada, C/ Ramón y Cajal, Granada, Spain
(3) Dept. Civil & Environmental Engineering, University of California, Davis, USA
(4) Dept. Civil Engineering, University of Granada, Campus de Fuentenueva, Edificio Politécnico, Granada, Spain
(5) Research Center for Information and Communications Technologies, University of Granada (CITIC), C/ Periodista Rafael Gómez Montero, 2, Granada,Spain
(6) Tahoe Environmental Research Center, USA

Abstract

A nested-grid approach with both normal and tangential velocity boundary conditions for 3-dimensional finite-difference, semi-implicit hydrodynamic models with Cartesian grid is evaluated. The nested implementation results show the same results that a non-nested semi-implicit implementation when both the inner and outer grids have the same resolution. Two kinds of tests applied to three different examples validate and demonstrate the excellence of the implementation. The examples are a synthetic rectangular basin with a constant wind, a real river model (Sacramento River, USA) and a real lake model (Lake Tahoe, USA). Simulation results of the real models are compared to sensor measurements in order to demonstrate the accuracy and applicability of the nested model implementation. The performance evaluation shows a dramatic improvement in memory requirements and simulation time. This work also evaluates the influence of the tangential velocity boundary conditions in the simulations (result quality and execution time), showing the impact on the results' quality when very strong currents, lateral circulations and/or vortices exist.

Keywords: model validation; nesting; shallow water equations; tangential velocity; real test models

Highlights

• A nested-grid implementation for 3D hydrodynamic models was evaluated and validated in two real applications • The inclusion of tangential velocities in the nested boundary conditions highly affects result quality when very strong currents, lateral circulation and/or vortices exist • The memory requirement is drastically reduced by using both nesting and a linear data representation that avoids storing dry cells.

* Corresponding autor. Tel: +34958241775. E-mail address: marioa@ugr.es (Mario Acosta)

1. Introduction

In the last decade, considerable progress has been made in the development of three-dimensional (3D) transport and mixing models which, based on the numerical solution of the Shallow-Water Equations (SWE), are capable of resolving with reasonable accuracy and computational cost *large-scale* physical processes in rivers, lakes and reservoirs ([1-5]). These models can also potentially be used to simulate *local-scale* processes, such as near-shore processes, where detailed topography and large changes in vorticity produce changes over small spatial scales, which requires high resolution grids to resolve. The challenge is that the high resolution grid needed to simulate local-scale processes requires disproportionately large amounts of CPU time and memory. Long simulation times are unacceptable when these models are part of decision support systems where, multiple simulations need to be run, or when the duration of a simulation exceeds the time period within which a result is required.

Unstructured or structured grid models could be used to conduct simulations of large basin-scale and local-scale processes. Unstructured models use grid cells of varying shapes and sizes that are pieced together to better represent topographic and bathymetric complexity. Small cell size can also be utilized where the local-scale processes are represented, increasing cell size away from the zone of interest. These models, however, are more computationally expensive than structured grid models ([6]). The algorithmic details are more complex than with structured grids, and the results are extremely sensitive to the quality of the generated mesh. Many important related physical processes (for example moist convection or suspended sediment transport) cannot be represented in an immediate and simple way as can be done with structured grids ([7]).

Many studies in shallow water modeling have used finite-difference, structured Cartesian grid models with very satisfactory results ([2,3,7,8]). Grid generation tasks and the implementation of the numerical solution are simpler when compared with unstructured approaches. Local-scale processes can be simulated using a high resolution grid covering the entire domain. However, this comes at a very high-computational cost. Alternatively, nested-grid models can be used at much lower computational cost in oceans ([8,10]), lakes ([3]) and rivers ([11]). In nested grid models, a higher resolution model (the inner model), is used to simulate the local-scale processes in a target zone. This inner model is embedded within a coarser resolution model (the outer model) that simulates the basin-scale processes. This approach allows for both the representation of

small scale mixing and transport processes, as well as the required resolution of small scale topographic and bathymetric features. The exchange of information between the outer and inner models becomes the critical task on which the quality of the solution depends.

Two approaches have been used to exchange information between the components of a nested-grid model. In conventional *one-way nesting* ([3,8,11-13]), the fine-resolution inner model is forced by the solution of the outer model, which is used to provide open boundary conditions. Alternatively, *two-way interaction* ([14-17]) may be used between the inner and outer models. This approach adds feedback from the inner model to the outer model, with the intention that the outer model benefits from the increased accuracy of the solution yielded by the inner model. Two-way interaction requires more execution time (computation and communication time) and does not always improve the results ([18]).

The exchange of information from outer to inner model (carried out in both one-way and two-way nesting) usually includes velocities, active scalar concentration (e.g. temperature, salinity or suspended sediment concentration), non-active scalar transport (e.g. chlorophyll concentration, tracer concentration) and water surface elevation. Many models ([13,15,17,19]) transfer normal velocity components to ensure that mass and momentum diffusion fluxes through the nested boundary are consistent, but they do not transfer tangential velocities. While some models ([8,14]) do transfer tangential velocities, they do not study its influence in the result quality and computational time. However, as is shown here, the absence of tangential velocities in the boundary conditions could be a source of error, especially, when the currents and lateral circulation are strong and/or features such as vortices exist.

A nested-grid one-way implementation for a semi-implicit finite-difference second-order Cartesian grid approach for the 3D-SWE (called Si3D [5]) is here evaluated and validated. The memory requirement is drastically reduced by using both nesting and a linear data representation that avoids storing dry cells. Two kinds of tests applied to three different examples validate the implementation and demonstrate the excellence of the results. The examples are:

- A synthetic rectangular basin with a constant wind, which demonstrates that the hydrodynamic fields in the inner and outer models are the same.

- Sacramento River (USA). This model is being used to understand the influence of river dynamics on the migration of salmon and to reproduce the lateral circulation in the area of meanders.

- Lake Tahoe (USA). This model is being used to study the transport of contaminants and planktonic larvae in the near-shore (littoral) zone.

The use of high resolution grids involves a serious computational cost for real models. This high computational cost prevents to predict in advance the migration of salmon in Sacramento River or the impact of contaminants and invasive species in Lake Tahoe. This happens due to the huge number of operations and the large storage memory required in 3D, semi-implicit, second order models, even when storing dry cells is avoided; for example, Lake Tahoe high resolution models need a computer with more than 12 GB of memory and Sacramento River high resolution models need more than 4GB of memory, even avoiding storing dry cells. Besides, when the sequential implementation is executed in an entry-level server, such as the Intel® Xeon® CPU L5506 core (4MB cache, 2.13 GHz, 4.80 GT/s Intel® QPI) with 16 GB of memory, Lake Tahoe high resolution model finishes 20 times after the end of the simulated period while Sacramento River high resolution model finishes nearly 3 times after. We have developed a hybrid shared and distributed memory parallel implementation with very good results for middle resolutions in cluster computers with multicore entry-level nodes, but with poor results for the high resolution needed in local-scale process simulations [18]. In order to deal with higher resolution models a nesting procedure is here used. Moreover, the real examples illustrate the importance of tangential velocities communication from outer to inner model. Lake Tahoe's tangential velocities are generally small compared to other forces, while in Sacramento River, due to strong currents and lateral circulation, they are much stronger.

This manuscript is organized as follows. Section 2 describes physical and computational characteristics of the Si3D model and the nesting approach used. Section 3 validates the nested implementation with two kinds of tests and both with synthetic and real examples, demonstrates the influence of tangential velocities in the simulations and evaluates the implementation performance. Finally, the last section summarizes the conclusions.

2. Si3D and the nesting approach

The finite-difference semi-implicit hydrodynamic and transport 3D Cartesian model used in this work was initially proposed for estuarine circulation [5] and it is also being used and validated in lakes and rivers [7]. In this work, for example, the nesting approach is validated with lake and river models. Si3D is based on the numerical solution of the 3D-SWE ([5]), the simplified form of the Reynolds averaged Navier-Stokes (RANS) equations. The governing equations can be written as

$$\frac{\partial u}{\partial x}+\frac{\partial v}{\partial y}+\frac{\partial w}{\partial z}=0 \tag{1a}$$

$$\frac{\partial \zeta}{\partial \mathrm{t}}+\frac{\partial}{\partial x}\left[\int_{-H}^{\zeta} u dz\right]+\frac{\partial}{\partial y}\left[\int_{-H}^{\zeta} v dz\right]=0 \tag{1b}$$

$$\frac{\partial u}{\partial t}+u\frac{\partial u}{\partial x}+v\frac{\partial u}{\partial y}+w\frac{\partial u}{\partial z}-fv=-\mathrm{g}\frac{\partial \zeta}{\partial x}+\frac{g}{\rho_0}\int_z^{\zeta}\frac{\partial \rho}{\partial x}dz' + \frac{\partial}{\partial x}\left(K_H\frac{\partial u}{\partial x}\right)+\frac{\partial}{\partial y}\left(K_H\frac{\partial u}{\partial y}\right)+\frac{\partial}{\partial z}\left(K_V\frac{\partial u}{\partial z}\right) \tag{2}$$

$$\frac{\partial v}{\partial t}+u\frac{\partial v}{\partial x}+v\frac{\partial v}{\partial y}+w\frac{\partial v}{\partial z}+fu=-g\frac{\partial \zeta}{\partial y}+\frac{g}{\rho_0}\int_z^{\zeta}\frac{\partial \rho}{\partial y}dz' + \frac{\partial}{\partial x}\left(K_H\frac{\partial v}{\partial x}\right)+\frac{\partial}{\partial y}\left(K_H\frac{\partial v}{\partial y}\right)+\frac{\partial}{\partial z}\left(K_V\frac{\partial v}{\partial z}\right) \tag{3}$$

$$\frac{\partial s}{\partial t}+\left[\frac{\partial (us)}{\partial x}+\frac{\partial (vs)}{\partial y}+\frac{\partial (ws)}{\partial z}\right]= \frac{\partial}{\partial x}\left(D_H\frac{\partial s}{\partial x}\right)+\frac{\partial}{\partial y}\left(D_H\frac{\partial s}{\partial y}\right)+\frac{\partial}{\partial z}\left(D_V\frac{\partial s}{\partial z}\right)+\frac{1}{\rho c_p}\frac{\partial I}{\partial z} \tag{4}$$

$$\rho=\rho(s) \tag{5}$$

These equations comprise the 3D-SWE. They express the physical principles of conservation of mass for an incompressible fluid (Eqs. 1a-b), conservation of momentum (Eqs. 2-3) and conservation of energy (Eq. 4). The *velocity* components in the *x*, *y*, and *z* directions are denoted by *u*, *v*, and *w*, *t* is time, *f* is the *Coriolis parameter*, *g* is the *acceleration due to gravity*, ρ represents *water density* variation with respect to a mean reference value ρ_0, ζ is the *water surface elevation* above an undisturbed level that can be chosen as *z=0*, and *-H=-H(x,y)* is the depth of the bottom boundary measured from the undisturbed free surface *z = 0*. Eq. 1a is the three-dimensional form

of the *continuity equation*, while Eq. 1b results from 1a by integration over the water depth, accounting for the kinematic boundary condition at the free surface and is the equation governing the free surface position. The integral terms in Eqs. 2-3 are referred to as *baroclinic (pressure gradient) terms*. The water surface slope terms in Eqs. 2-3 are referred to as *barotropic (pressure gradient) terms*. Eq. 4 represents the transport equation for active scalar concentration fields, *s* (temperature or salinity or sediment concentration). The last term in Eq. 4 is a source-sink term representing the surface heat flux, and c_p is the *heat capacity of water*. The coefficients K_H and K_V represent the horizontal and vertical turbulent transport coefficients for momentum (or kinematic *eddy viscosity*), and D_H and D_V are the horizontal and vertical turbulent transport coefficients for active scalar concentration (*eddy diffusivity*). Eq. 5 is a state equation which links active scalar concentration and density, ρ.

The governing equations are first posed in layer-averaged form by integrating over the height (*h*) of a series of horizontal layers separated by level planes. The layer-averaged form of the equations is discretized using a semi-implicit, three-level, iterative leapfrog-trapezoidal finite-difference algorithm (with second-order accuracy) on a staggered Cartesian grid. The calculations to obtain the finite-difference form and the layer-averaged form of the governing equations are detailed in [5]. The layer-integrated volumetric transports replace velocities as the dependent variables so that the depth-integrated continuity equation that is used in the solution for the water surface elevation is linear. Volumetric transports are computed explicitly from the momentum equations (Eqs. 2 and 3). The resulting method is mass conservative, efficient, and numerically accurate ([5]).

The semi-implicit approach (see [20]) is based on treating implicitly the barotropic pressure gradient in the momentum equations and the velocity divergence in the continuity equations, in order to avoid time-step limitations due to gravity-wave Courant-Friedrichs-Levy CFL condition. All other terms, including the baroclinic pressure gradients associated to spatial variations in density, are treated explicitly. Laplace operators are used to represent mixing. Constant mixing coefficients are used to parameterize the effect of horizontal eddies or vortexes. A two-equation turbulence model calculates the vertical eddy coefficients of mixing. Computations in each iteration proceeds on a water column-by-water column to assemble a five-diagonal

system of equations for water surface elevation ζ. This system is then solved using a preconditioned non-symmetric conjugate gradient method, which is an iterative method (hence approximate) that converges to the correct value within a tolerance. Horizontal velocities are recovered from the updated values of ζ. The vertical velocity, w, is then updated using the continuity equation (Eq. 1a). The active scalar concentration is solved after the hydrodynamic variables are determined.

The 3D model variables are stored in one- or two-dimensional arrays in order to decrease memory requirements. 1D arrays store 2D variables defined in x and y directions, such as water surface elevation ζ. 2D arrays store 3D variables defined in x, y and z directions: first dimension for x and y, second for z. This implementation improves the memory requirements and the data locality by not reserving space for dry columns. Neighboring north, south, east and west water columns are accessed using 4 arrays of one dimension (one for each direction). These arrays avoid the extra operations needed to obtain neighbor columns, while take up an imperceptible memory space; for example, these arrays take up 0.05% of the total memory required in Lake Tahoe model and 0.02% in Sacramento River model.

2.1 Nesting procedure

Figure 1 presents a schematic set up of a nested solution for the problem of simulating circulation and transport in a rectangular-shape basin. However, the nesting approach used allows irregular cuts, to adapt to the region of interest and remove the deep areas, which increase the computational cost. The Figure 1 example resolves the local-scale physical processes in the sub-basin or sub-domain formed by the northeastern corner; those processes are partly driven by the large-scale basin circulation. The basin is discretized using a structured grid with square cells of horizontal size Δx_{og}. The boundary that separates the sub-basin from the rest of the lake will be referred to as the IO (Inner/Outer) boundary. The sub-basin in the inner model is discretized with cells of size $\Delta x_{ig} \leq \Delta x_{og}$. Therefore, the number of water columns of the inner model, N_{im}, will be larger than the number of columns of the outer model in the sub-basin N_{om}, being $N_{im} = (\Delta x_{og}/\Delta x_{ig})^2 \, N_{om}$. The ratio $\Delta x_{og}/\Delta x_{ig}$ will be the grid refinement r_g. Column vertical resolution can vary among columns. The vertical resolution of the inner and outer grids is equal in the implementation.

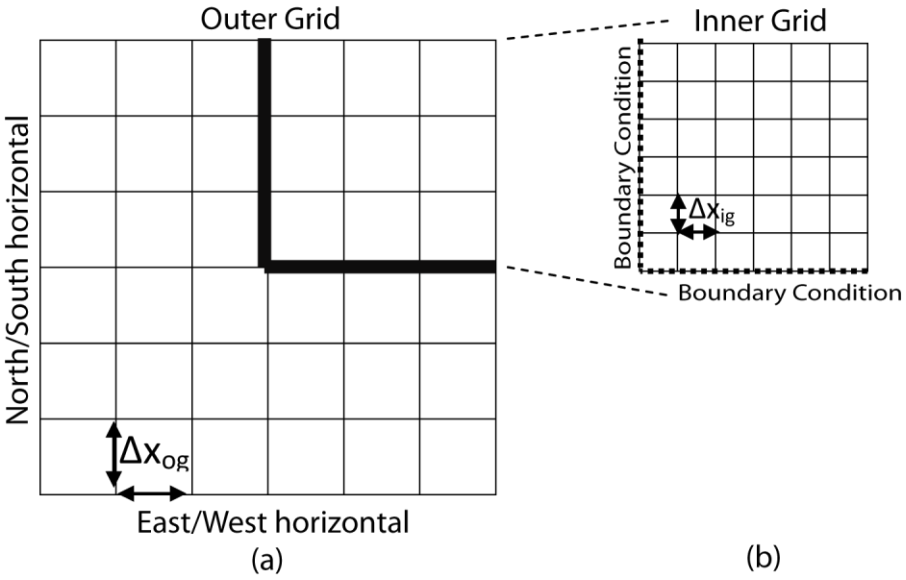

Figure 1. Nesting grid example, (a) outer grid model or basin where Δx_{og} is East-West and North-South horizontal resolution and (b) inner grid model or sub-basin where horizontal resolution Δx_{ig} is half the outer model horizontal resolution.

The nested procedure consists of a set of rules defined to exchange information across the boundaries that separate the inner model and the outer model (here on referred to as the IO boundary). These rules include (1) the identification of the variables whose values need to be exchanged across the boundary, so that, in the process of assembling the equations and matrices that govern the solution in the inner sub-domain, all necessary values are known; (2) an appropriate interface between the outer and the inner model must be designed and implemented so that there is an exact and univocal correspondence between grid indexes and discrete variables between the inner and outer models, (3) instructions on how the equations need to be assembled so that the inner and outer model solutions coincide in the inner sub-domain if both inner and outer models use the same space-time resolution. Details of the development of the nesting procedure are given in Acosta et al. (2013, MAMERN).

Independently of whether the nested solution is implemented using a one-way or a two-way approach, the inner model needs to exchange information with the outer model along the IO boundaries. In the simulations presented here, the outer model exchanges information (scalar concentration, height, normal and tangential velocities and volumetric transports) with inner model at each time step Δt and both models have

the same time step, one acceptable to inner model. However, the time steps of inner and outer models (Δt_{im} and Δt_{om}) do not need to be the same. In fact, Δt_{om} could be larger than Δt_{im} given the larger size of the grid cells. The lapse of time between consecutive communications could also expand to several time steps of the outer model and the IO boundary information could be interpolated in time, letting outer model simulate ahead of time. Preliminary tests showed that the best results were obtained when the time steps are the same in the outer and inner models, and the communications are conducted once per time step. However, communication every few time steps produced very similar results, and reduced the amount of data exchange. This can be taken into account when the user needs to improve the computational cost without losing too much quality in the results.

3. Model evaluation

Two kinds of tests and three examples (a synthetic rectangular basin with a constant wind, Sacramento River and Lake Tahoe) are used to validate and evaluate the model. The tests are:

A. A test with outer and inner models with the same resolution is applied to the three examples ($r_g=1$). This test is designed to demonstrate that the inner and outer domains are coupled seamlessly. In this test, the velocity fields (u (E-W), v (N-S) and w (vertical)), water surface elevation (ζ) and temperature (s, active scalar concentration) of both models are compared.

B. A test with an inner model with higher resolution than the outer model is applied to the real examples ($r_g>1$). The simulation results of the higher resolution inner model are compared to available sensor measurements, in particular, flow data in Sacramento River and profiles of horizontal velocity in Lake Tahoe, in order to demonstrate the implementation accuracy and the hydrodynamic model accuracy. Performance (memory and time) improvement is also analyzed. Performance has been evaluated in a computer with characteristics (processor microarchitecture, processor normal clock speed, cache memory size and architecture, point-to-point memory communication instead of bus memory communication, speed of memory communication etc.) of a conventional low-priced and low-power consumption entry-level server. The computer has an Intel® Xeon® CPU L5506 processor (4 cores, 4MB cache, normal clock speed

2.13 GHz, 4.80 GT/s Intel® QPI – 19.2GB/s max. memory bandwidth, and low thermal design power of 60W) and 16 GB of memory (the Intel recommended customer price is $423).

In test A the differences between the outer and inner model solutions after multiple simulation time steps are taken as a measure of the validity of the nested algorithm implementation. This differences were quantified using the root mean squared error (RMSE) and a normalized root-mean-squared error (NRMSE), defined as follows

$$\mathrm{RMSE} = \sqrt{\frac{\sum_{l=1}^{N_{im}} \left(x^{1,l} - x^{2,l}\right)^2}{N_{im}}} \tag{15}$$

$$NRMSE = \frac{RMSE}{x_{max} - x_{min}} \tag{16}$$

In these equations, x^1 is a variable in the outer model and x^2 the same variable in the inner model; x_{max} and x_{min} are its maximum and minimum values both in outer and inner model. N_{im} is the total number of water columns in the inner model. The RMSE has been used in Test B too, in that case to quantify the differences between the sensor measurements and the simulations results, where x^1 represents the sensor measurements, x^2 the simulation results of the higher resolution inner model and N_{im} is the total number of experimental data collected along the time.

In the first example, the domain is a flat bottom rectangular basin with a small number of grid cells (Section 3.1). The sub-basin is the southern end of this basin. In the second (Sacramento River), the sub-basin is a curve of the river that presents high values of velocities (normal and tangential) and lateral circulation, producing vortexes in the sub-basin frequently (Section 3.2). The last example (Lake Tahoe) resolves the circulation and transport patterns in the lake's near-shore regions (Section 3.3). The two real examples also illustrate that the construction of the IO Boundary is a non-trivial task because the chosen implementation affects the quality of the results significantly as shown by the influence of tangential velocities in Sec. 3.4.

3.1. Case 1: Rectangular flat bottom basin.

Test A was applied to a rectangular basin aligned in the N-S direction, with a length of 99m and a width of 5 m (see Figure 2). It has a constant depth of 10 m. The basin is discretized using square cells of size Δx = 1 m and Δy = 1 m, and a vertical dimension of Δz = 0.5 m. The inner grid covers the southern 19 m of the channel. The model is forced with a constant southern wind, and the period of time simulated is 10 days. The time step is set to 5 seconds. Every 20 hours, all the variables (u, v, w, ζ and s on the free surface plane) were output, and the outer and inner solutions in the southern end of the basin were compared.

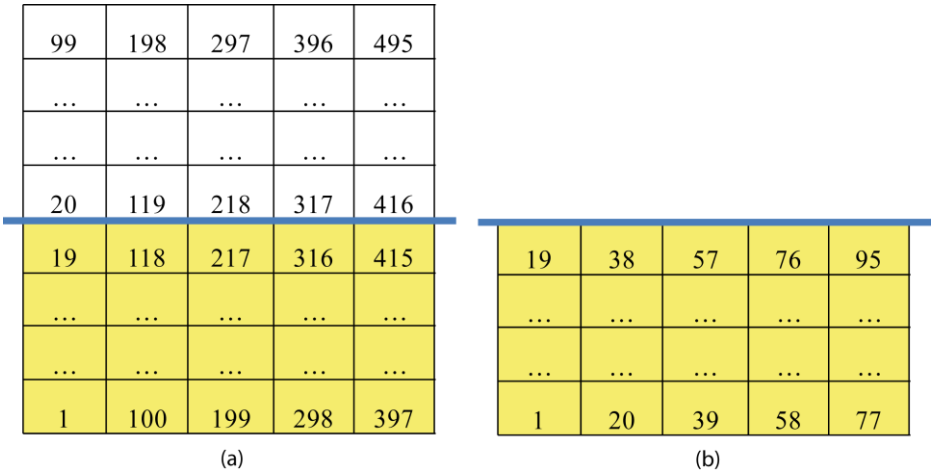

Figure 2. A rectangular channel: (a) outer model and (b) inner model

The normalized error is obtained during the simulations for all variables in all output epochs (every 20 hours). Besides, the water volume of the outer and inner models in the coincident zone is compared in order to demonstrate the volume conservation between the outer and inner models. This volume is calculated multiplying the sum of ζ by the product $\Delta x \times \Delta y$, being Δx and Δy the horizontal dimension of the cells. The NRMSE (Eq. 16) for all variables and the water volume comparison is less than 4% in all output epochs. The largest errors are for ζ (water surface elevation). This error is low and is due to the preconditioned conjugate-gradient method used to solve the five-diagonal system of equations for water surface elevation. An iterative method, such as the preconditioned conjugate-gradient, converges to the solution of the matrix problem with a much lower computational cost than direct methods. However, the solution of a direct method is exact, while the solution with an iterative method is approximate within a tolerance, which is set by the user. In real applications, it is not efficient to use direct methods to solve the very large systems of equations that are

assembled, but in simplified and very small problems, the direct methods can be used to eliminate the approximation error in the solution of the matrix. Given the size of the problem being solved in this test case, the system of equations for free surface elevation can be solved with a reasonable cost using a direct method in both outer and inner grid. In this manner, we eliminate the solution of free surface elevation as a source of error. The RMSE for u, v, w, ζ and s are then all zero. These results demonstrate that the nested approach here proposed does not introduce errors.

3.2. Case 2: Sacramento River

The Sacramento River (Figure 3(left)) model is being used to study the influence of river dynamics in the migration of salmon and, in particular, how lateral circulation in the area of bends influence salmon drift toward the headwaters, since many of these salmon begin or end in this type of river structures. The fluvial dynamics in the lower of the river is influenced both by the *flow* from the middle stretch of the river and its tributaries, as well as by *tidal* dynamics. Reproducing the lateral circulation and small-scale vortices in the area of meanders requires a high resolution grid (a bathymetry with square columns of 2m, the maximum resolution available provided by the United States Geological Survey (USGS), is enough), which made it computationally unfeasible. The nested procedure here proposed allows resolving the problem with an acceptable computational time by using a high resolution grid just in the meander area under study, Clarksburg Bend (Figure 3(right)). The data presented here are the results in this meander in the outer and inner models. The outer domain includes the whole basin (shown in Figure 3(left)) and is discretized using grid cells of size 10m x 10m in the horizontal plane while the inner domain uses 10m x 10m (Test A) or 2m x 2m (Test B) cells, i.e. r_g=1 or r_g=5, respectively.

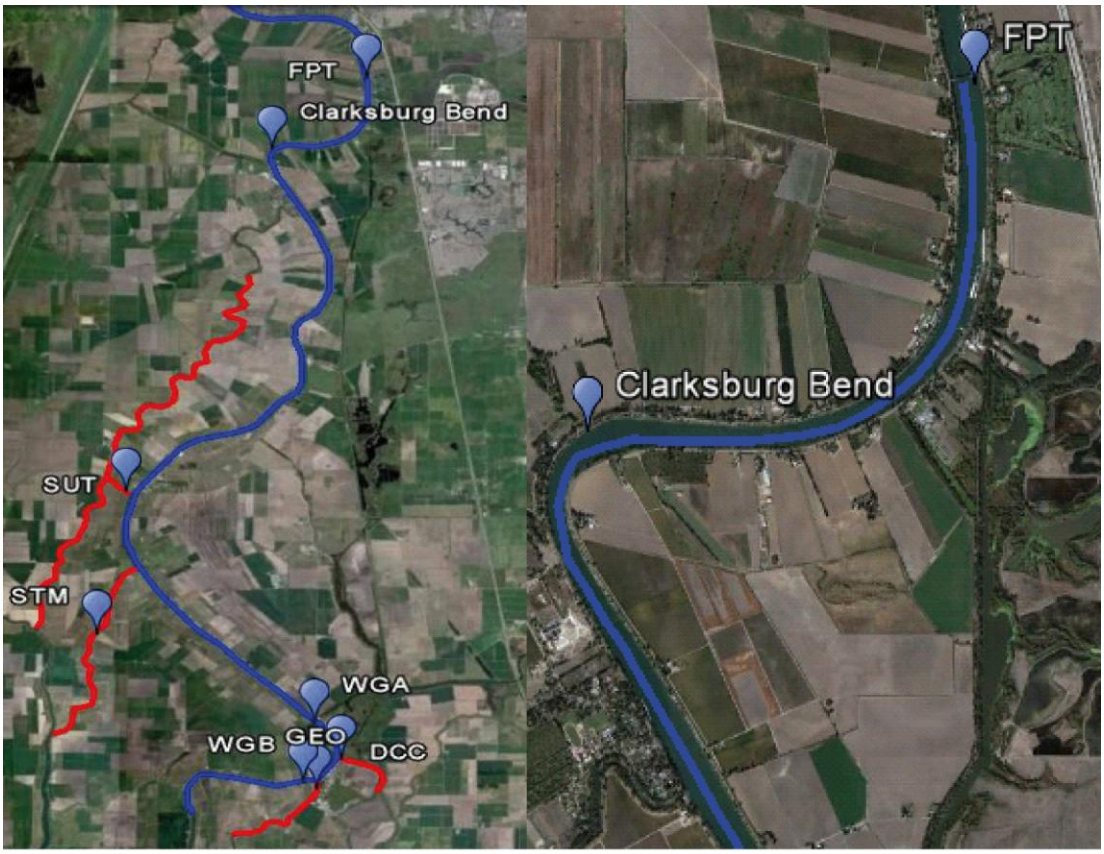

Figure 3. Sacramento River hydrodynamic model domain: outer domain (left) and inner domain (right). The river is shown in blue and tributaries are shown in red. Markers show the location of USGS gaging stations used as model boundary conditions and internal validation points.

The boundaries of the outer domain were chosen to match the location of existing USGS gaging stations (FPT, WGA, WGB, SUT, STM, DCC and GEO, Figure 3(left)). Inflows were forced at model boundaries matching the locations of FPT, SUT, STM and DCC, according to observations collected in each of these gaging stations, in a given time period. Free surface elevations at the other three model boundaries were forced to vary according to observations collected in WGA, WGB and GEO gaging stations respectively. Temperature comparison is not provided for Sacramento River, because it was kept constant (with a uniform temperature equal to 8º C typical of the winter period) in all the simulation due to the negligible variations in Sacramento River temperatures in the month studied (January). Sacramento River temperatures normally begin to decline in October, remain uniform from December to March, and begin to increase in April. The model was simulated during a period of time (simulation or study period) of 10 days in 2009 starting on January 8th and ending on January 17th.

Test A. Velocity field and water surface elevation comparison - All the domain has been compared between inner and outer models in the area where both coincide (Figure 3(right)). Figure 4 compares, for each variable evaluated, the value obtained by the solution of inner model (Figure 4, y-axis) with the solution obtained by outer model (Figure 4, x-axis) for all output epochs at the same time. If the solution obtained by outer and inner model is exactly the same, its value is placed on the dashed line. If the outer model solution is higher than the inner model, the point is placed in the lower triangle while if it is lower, it is placed in the upper triangle. The compared variables are horizontal velocities (*u* and *v*) vertical velocity (*w*) and water surface elevation (*ζ)*. The NRMSE (Eq. 16) averaged over the simulation time is 4%, 2%, 3% and 0.2% for *u, v* , *w* and *ζ* respectively. Finally, the sum of *ζ* is used to check for volume conservation, applying the same procedure as in the case of rectangular flat bottom basin to obtain volume (*(Σζ) × Δx × Δy*). The RMSE (Eq. 15) averaged over time is 0.19m^3, which represents 0.1% of the average volume over the simulation time measured in the coincident area.

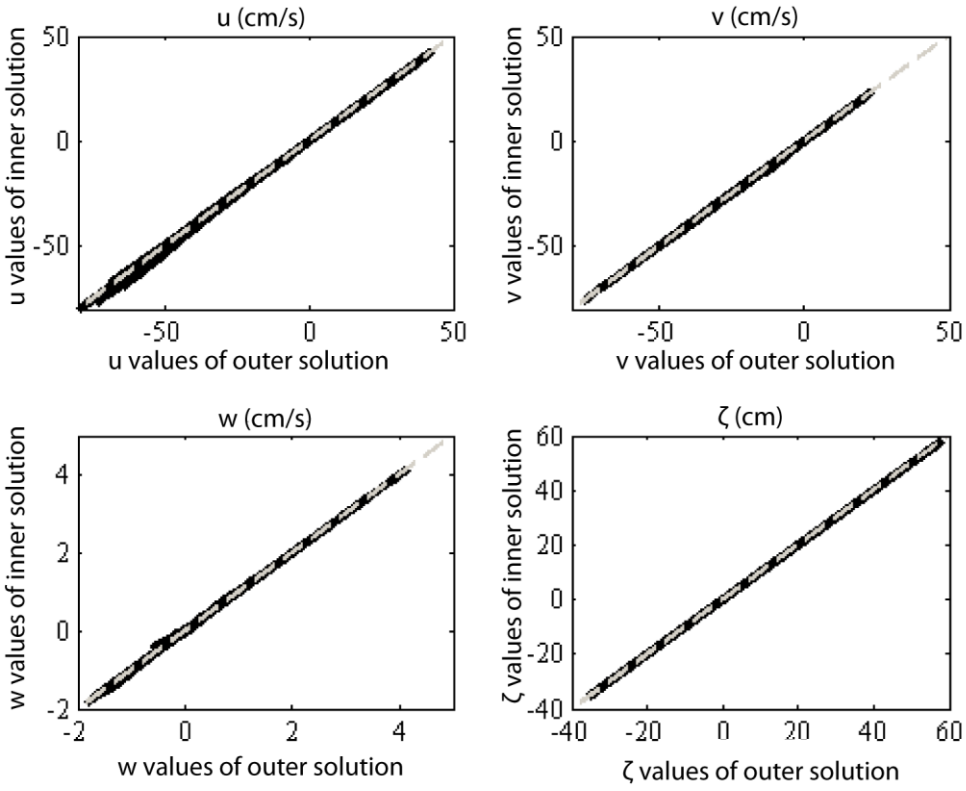

Figure 4. Sacramento River: *u, v, w and ζ,* compared between inner and outer model solutions in all the domain. Each point represents the value obtained by inner model

solution (y-axis) against the solution obtained by outer model (x-axis). If both solutions coincide, the point is located on the dashed line.

Test B. Comparison with sensor measurements and performance - The flow (current) is calculated in a section of the river in the curve (Figure 3(right)). This computed flow is then compared with flow data supplied by the USGS field station at FPT (Figure 3(left)), measured with a short-range Nortek Acoustic Doppler velocity meter and Current Profiler (ADCP) with upward-looking stage sensor, giving a RMSE of ~21m^3/s (5% of maximum flow measured in FPT). However, as Figure 5 shows, these deviations occur especially during periods of high and low tides (maxima and minima in Figure 5); in fact, Clarksburg Bend is located downstream of FPT and therefore receives a greater influence of tidal dynamics than FPT, so these deviations are expected. A Goldin filter can be used to eliminate the tidal component of the results and obtain just the desired discharge component of the main river. With a Goldin filter, the RMSE is practically 0, as shown in Figure 6, (0.3m^3/s, which is 0.01% of the maximum flow measured in the field, FPT). Performance improves significantly by both storing just columns with water and applying the nested implementation. First, the memory requirement is reduced a 97.19% approximately by storing just columns with water. Second, by applying in addition the nested implementation, the memory is reduced, additionally, an 85%, and the sequential time is reduced an 82% in the test computer described above. These reductions allow the use a low-priced computer in the research or predictions (this also means low energy consumption). Moreover, it also allows running multiple simulations all at once in staffs' personal computers, or in a low-priced cluster.

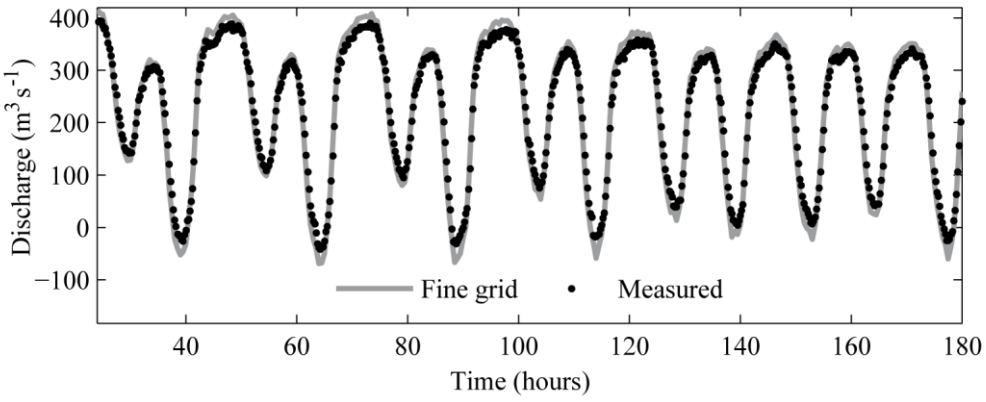

Figure 5. Sacramento River: Simulated discharges (m^3/s) at a section located in the bend compared to measured values at FPT gate by ADCP.

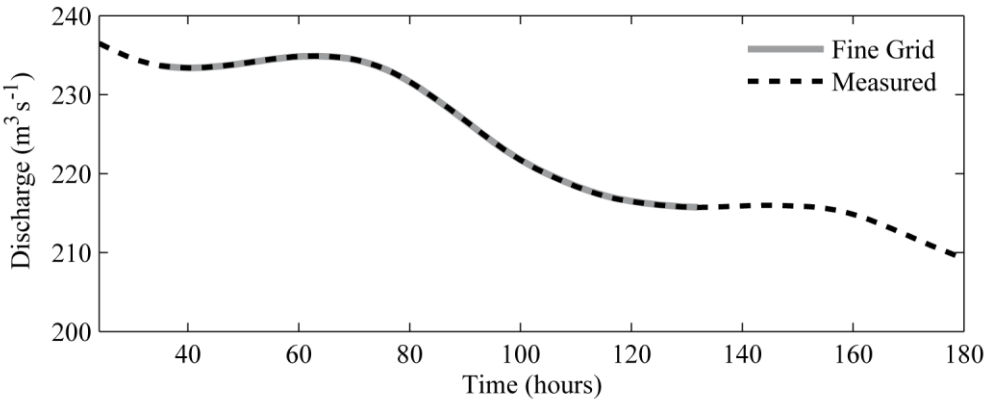

Figure 6. Sacramento River: Discharge after applying a Goldin filter to remove the tidal component and obtain just the discharge component in the results (m^3/s).

3.3. Case 3: Lake Tahoe

The nested-grid approach is being used to resolve near-shore circulation in Lake Tahoe (Figure 7). The extraordinary variability of the physical environment in the near-shore makes the task of characterizing it by means of observations a challenge.

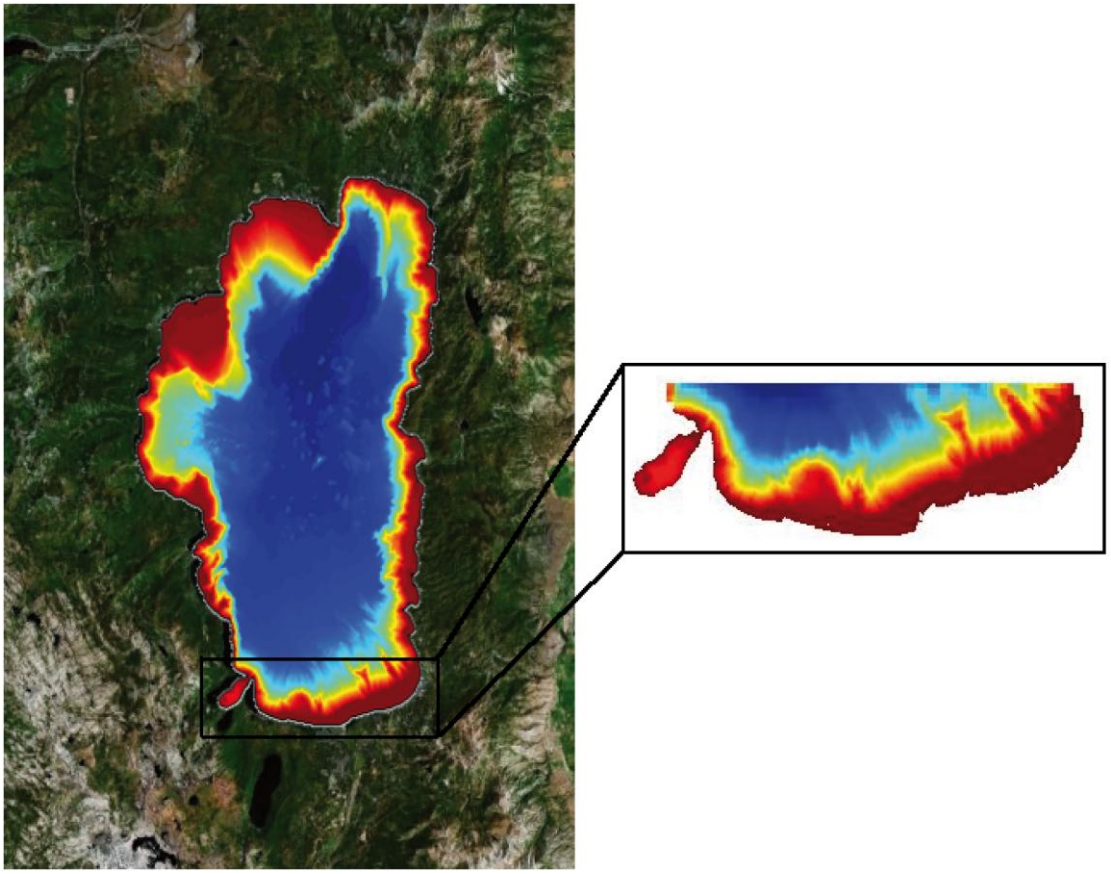

Figure 7. Lake Tahoe hydrodynamic model domain: outer model (left) and inner model (right).

Near-shore circulation can be used in different studies. For example, in Lake Tahoe, it is going to be used to develop a long-term risk assessment of Asian clam growth, spread and impact. In this study, the near-shore circulation can be used to develop a transport model of Lake Tahoe to characterize the pathways of transport of young life stages of Asian clams from the existing beds to other near-shore areas. To achieve this goal, a high resolution model must be used where fine-scale information is needed (such as in the near-shore). The nested approach to develop a high-resolution transport model of the near-shore is justified because the high-resolution simulation of the whole lake (roughly 20 km x 30 km in the horizontal dimension and a depth of up to 500 meters in the vertical dimension) would require expensive computation hours in expensive and high energy consumption parallel computer platforms.

The selected study area for the observational experiments was the region adjacent to the largest urban area, South Lake Tahoe (Figure 7). This is where the greatest anthropogenic effects are known to occur and declining water quality has been measured ([21]). The outer domain is discretized using grid cells of size 100m x 100m in the horizontal plane, while the inner domain uses 100m x 100m (Test A) or 20m x 20m (Test B) cells, i.e. r_g=1 or r_g=5, respectively. The Lake Tahoe bathymetry data used for the present study was obtained from USGS (Figure 7). Notice the different resolution of the bathymetric information near the IO boundary on the north, and away from it. The vertical resolution is set up as layers with variable depth increasing from 0.5 m near the top to nearly 10 m near the bottom.

In the simulation, the model was forced (input data) using surface heat and momentum fluxes estimated from local atmospheric variables (short and long wave radiation, air temperature, relative humidity, and wind speed and direction) obtained from meteorological data. These data were taken primarily from meteorological stations maintained by the Tahoe Environmental Research Center (TERC). There are ten shoreline and on-lake meteorological stations. All stations provide a near-continuous record of wind magnitude and direction and air temperature. The model was simulated during a period of time (simulation or study period) in 2008 starting on July 22nd and finishing on July 31st.

Test A. Velocity field, water surface elevation and temperature comparison - All the domain has been compared between inner and outer model in the coincident area (Fig.

7(right)), both models with 100m square columns. The variables evaluated are horizontal velocities (*u* and *v*), vertical velocity (*w*), water surface elevation (ζ) and temperature (*s*). The results are similar to those obtained in Sacramento River. The NRMSE (Eq. 16) averaged over time is 2.5%, 1.7%, 0.8%, 1.7% and 0.9% for *u*,*v*, *w*, ζ and *s* respectively. Finally, the RMSE (Eq. 15) of the water volume ($(\Sigma\zeta) \times \Delta x \times \Delta y$) differences between outer-inner models, averaged over time, is $0.22m^3$ which represents 0.14% of the average volume over time measured in the coincident area.

Test B. Comparison with sensor measurements and performance - Near-continuous profiles of velocities (magnitude and direction) in 0.50 m vertical bins were observed with an ADCP. Equipment was deployed from July 28th (Julian day 209) to July 31st (Julian day 212) 2008 in the near-shore of the south region. The results of the high-resolution model (*u* and *v* horizontal velocity) were compared with the profiles of velocities measured by ADCP (Figure 8). As shown in the figure, the high-resolution model provides an accurate representation of the observations for the u velocity component and especially for the v velocity component. Performance improves significantly by both storing just columns with water and applying the nested implementation. First, the memory requirement is reduced a 34.8% approximately by storing just wet cells. Second, by applying in addition the nested implementation, the memory is reduced, additionally, a 92%, and the sequential time is reduced a 94% in the test computer. These reductions allow the use of the low-priced and low-power consumption test computer in the research or predictions in Lake Tahoe, but, due to the inner and outer grid size in this particular example, our parallel implementation [22] must be used in order to finish the simulation before the end of the simulation period (the test computer has 4 cores). Multiple nested-grids of the lake can be simulated all at once in the in staff's personal computers, or in a low-cost cluster.

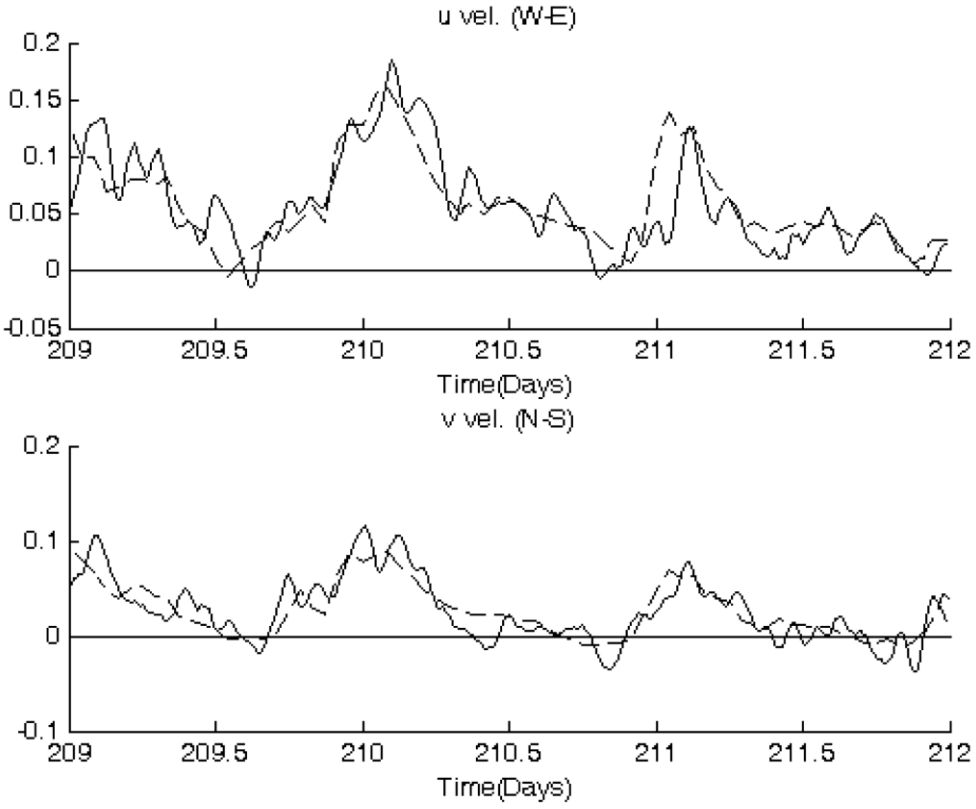

Figure 8. Lake Tahoe: u (W-E) and v (N-S) horizontal velocity in a point in the topmost layer in the simulation period between July 28th, 2008 (Julian day 209) and July 31th, 2008 (Julian day 212). Experimental data measured by ADCP and simulation data of the high resolution model (dashed line).

3.4. Influence of tangential velocities in Lake Tahoe and Sacramento River.

The correct construction of IO Boundary is a fundamental task to get a correct coupling between outer and inner model. It is necessary to prevent a source of error that may impair the quality of the results of the nested model, and to avoid problems in the conservation of mass and volume of the nested model. In the variable dependence graphs for grid points next to the IO Boundary shown in Section 2, the two velocity components (normal and tangential) are among the variables that must be communicated. Some nested implementations ([13,15,17,19]) use just the normal component in the construction of IO Boundary, probably because tangential values for the simulated models are very small compared to other forces and their absence in the construction of IO Boundary does not affect the results, as is the case of the nested area simulated in Lake Tahoe, but in models such as Sacramento River, with high values of

lateral circulation and flow directional gradients in the nested area (a curve in the domain, Figure 3(right)), the tangential velocities reach large values, being comparable to normal velocities. In this case, their absence in the IO Boundary construction can lead to cumulative errors in the nested model and a consequent loss of quality in the results.

To assess the importance of a complete communication of the two velocity components in the construction of the IO Boundary in different models, the velocity field and water surface elevation (ζ) comparison (Test A) made above was repeated not communicating the tangential velocity component this time (the rest of the variables are sent as in the previous case).

Table I. NRMSE (%) in all the inner domain averaged over time for Lake Tahoe and Sacramento River, comparing the construction of IO Boundary with and without the component of tangential velocity.

Variable	Tahoe – Using tangential velocities in IO Boundary	Tahoe – Without tangential velocities in IO Boundary	Sacramento – Using tangential velocities in IO Boundary	Sacramento – Without tangential velocities in IO Boundary
Vel. u (W-E)	2.518	3.146	4	34
Vel. v (N-S)	1.783	2.518	2	17
Vel. w (vert.)	0.885	0.977	3	28
ζ (wse)	1.731	2.172	0.2	1
s (temp.)	0.902	0.994	Not measured	Not measured

In the results obtained, in both real examples the differences are greater when the tangential velocities are not transferred (Table I). The differences are barely significant in Lake Tahoe (Table I, columns 2 and 3). However, in Sacramento River, differences are very important (Table I, columns 4 and 5 and Figure 9), especially in velocity variables. Therefore, the results show that the use of the tangential velocities deserves attention. The simulation time is imperceptibly affected (for example, it increases just a 0.6% in Lake Tahoe), so the model can be programmed to always use them, freeing the researcher or end-user from deciding about it.

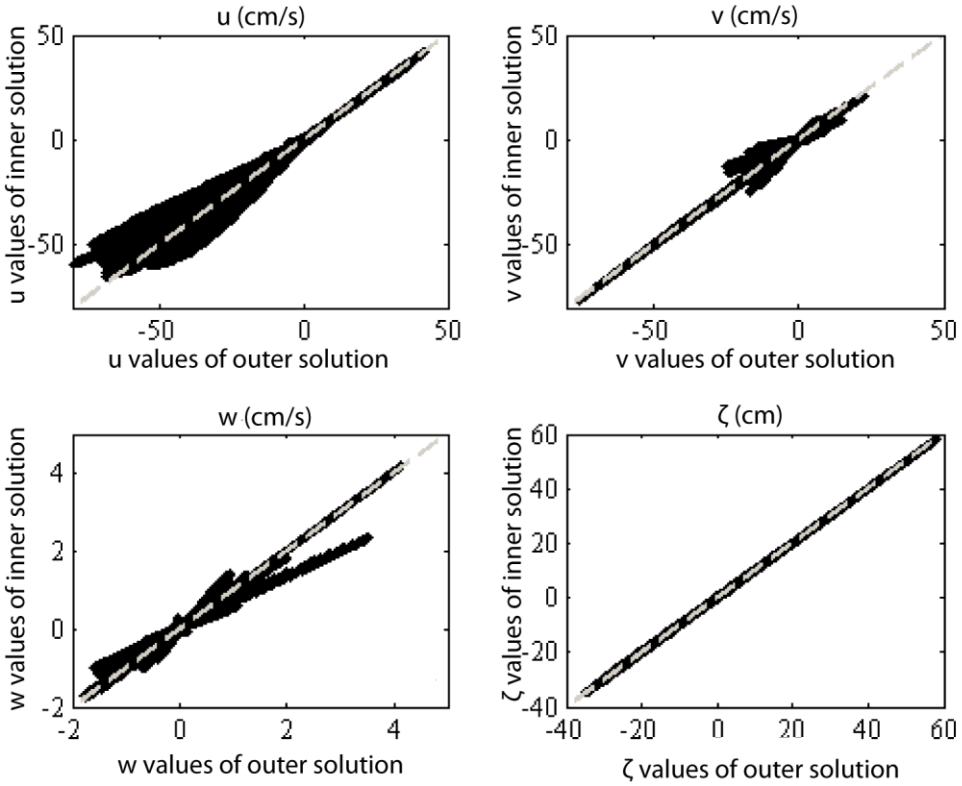

Figure 9. Sacramento River with IO boundary built without tangential velocities: *u*, *v*, *w and* ζ, compared between inner and outer model solutions in the whole domain. Each point represents the value obtained by inner model solution (y-axis) against the solution obtained by outer model (x-axis). If both solutions coincide, the point is located on the dashed line.

4. Conclusions

This work presents the evaluation and validation of a nested grid approach with both normal and tangential velocity boundary conditions for 3D finite-difference hydrodynamic models with Cartesian grid. The Cartesian grid memory requirements are drastically reduced by using nesting and a linear data representation that stores just information of columns with water. This made the implementation suitable for simulations of irregular targets, such as rivers.

The evaluation and validation of the test results show that:

- The inner and outer domains are coupled seamlessly in the implementation (Tests A in Section 3). The nested approach proposed does not introduce

additional errors. The errors are due to the iterative method and the different inner and outer grid resolution.

- The nested-grid 3D finite-difference semi-implicit Cartesian model used and evaluated provides accurate simulation results using high-resolution grids, as shown by the comparisons with experimental sensor measurements (Tests B in Section 3). Simulation results provide an accurate representation of the sensor observations for the two real test models simulated, with almost zero errors in Sacramento River.

- Both normal and tangential velocity boundary conditions are needed in nested models with complex flow patterns in areas with high flow directional gradients because flows entering the nested grid under an angle can be represented accurately (Section 3.4). The inclusion of tangential velocities in the boundary conditions highly affects result quality when very strong currents, lateral circulation and/or vortices exist with negligible effect on processing time. Error percentages even of tens in Sacramento River have been obtained when they are not included. The influence of tangential velocities illustrates that the construction of the IO Boundary is a non-trivial task because the chosen implementation can affect the quality of the results notably.

- Performance improved significantly with the nested implementation proposed. A drastic reduction in both the memory occupied by data (85% in Sacramento River and 92% in Lake Tahoe) and in the simulation time (82% in Sacramento River and 94% in Lake Tahoe) has been achieved. These reductions imply that simulations can be executed in a low-priced and low-power consumption computer, or that multiple simulations can be run all at once on personal computers, or in a cluster of low-cost computers.

Acknowledgement

Bathymetry data were collected by the USGS California Water Science Center (USGS CWSC) using the USGS BathMapper software suite to measure bottom depths using downward looking ADCPs. A detailed summary of the bathymetry acquisition and DEM generation process can be found at: https://sites.google.com/site/bathmapperwiki/Home/bathymetry-surveys/northern-sacramento-river-detailed-modeling-survey-june---07.

This manuscript was in part prepared during a stay at University of California Davis funded by University of Granada (Department of Computer Architecture and Technology, CEIBioTIC, Vice-Rector's Office for Scientific Policy and Research, Escuela Internacional de Posgrado, Vice-Rector's Office for International Relations and Development Cooperation).The hospitality at University of California Davis is greatly appreciated. The first author was granted a scholarship by the University of Granada. Additional support for the Lake Tahoe case study was provided through a grant to the fifth author from the US Forest Service under the Southern Nevada Public Lands Management Act.

References

1. Acosta MC, Anguita M, Rueda FJ, Fernandez FJ. Parallel Implementation of a Semi-Implicit 3-D Lake Hydrodynamic Model. Proc. of the 2010 Int. Conf. on Comp. and Math. Methods in Science and Eng. (CMMSE) 2010; **IV**: 1026-1037.Almería (Spain).

2. Barth A, Alvera-Azcárate A, Rixen M, Beckers J. Two-way nested model of mesoscale circulation features in the Ligurian Sea. *Progress in Oceanography* 2005; **66**: 171-189. DOI:http://dx.doi.org/10.1016/j.pocean.2004.07.017.

3. Bonaventura L, Rosatti G. A cascadic conjugate gradient algorithm for mass conservative, semi-implicit discretization of the shallow water equations on locally refined structured grids. *International Journal for Numerical Methods in Fluids* 2002; **40**: 217-230. DOI:10.1002/fld.274.

4. Casulli V, Cheng RT. Semi-implicit finite difference methods for three-dimensional shallow water flow. *International Journal for Numerical Methods in Fluids* 1992; **15**: 629-648. DOI:10.1002/fld.1650150602.

5. Fox AD, Maskell SJ. Two-Way Interactive Nesting of Primitive Equation Ocean Models with Topography. *Journal of Physical Oceanography* 1995; **25**: 2977-2996. DOI:10.1175/1520-0485(1995)025<2977:TWINOP>2.0.CO;2.

6. Giunta G, Mariani P, Montella R, Riccio A. pPOM: A nested, scalable, parallel and Fortran 90 implementation of the Princeton Ocean Model. *Environmental Modelling & Software* 2007; **22**: 117-122. DOI:http://dx.doi.org/10.1016/j.envsoft.2006.05.024.

7. Griffies SM, Boning C, Bryan FO, Chassignet EP, Gerdes R, Hasumi H, Hirst A, Treguier AM, Webb D. Developments in ocean climate modelling. *Ocean Modelling* 2000; **2**: 123-192. DOI:doi:10.1016/S1463-5003(00)00014-7".

8. Harris LM, Durran DR. An Idealized Comparison of One-Way and Two-Way Grid Nesting. *Monthly Weather Review* 2010; **138**: 2174-2187. DOI:10.1175/2010MWR3080.1.

9. Heggelund Y, Berntsen J. A method for analysing nesting techniques for the linearized shallow water equations. *International Journal for Numerical Methods in Fluids* 2002; **38**: 163-185. DOI:10.1002/fld.215.

10. Hinterberger C, Fröhlich J, Rodi W. Three-Dimensional and Depth-Averaged Large-Eddy Simulations of Some Shallow Water Flows. *Journal of Hydraulic Engineering-asce* 2007; **133**: 857-872. DOI:10.1061/(ASCE)0733-9429(2007)133:8(857).

11. Huang A, Rao YR, Lu Y, Zhao J. Hydrodynamic modeling of Lake Ontario: An intercomparison of three models. *Journal of Geophysical Research: Oceans* 2010; **115**: - C12076. DOI:10.1029/2010JC006269.

12. Kolerski T, Shen HT, Knack IM. A Nested Model for River Ice Dynamics. Proceedings, 20th IAHR Ice Symposium 2010;Lahti, Finland.

13. Leon LF, Smith REH, Malkin SY, Depew D, Hipsey MR, Antenucci JP, Higgins SN, Hecky RE, Rao RY. Nested 3D modeling of the spatial dynamics of nutrients and phytoplankton in a Lake Ontario nearshore zone. *Journal of Great Lakes Research* 2012; **38, Supplement 4**: 171-183. DOI:http://dx.doi.org/10.1016/j.jglr.2012.02.006.

14. Paris CB, Helgers J, van Sebille E, Srinivasan A. Connectivity Modeling System: A probabilistic modeling tool for the multi-scale tracking of biotic and abiotic variability in the ocean. *Environmental Modelling & Software* 2013; **42**: 47-54. DOI:http://dx.doi.org/10.1016/j.envsoft.2012.12.006.

15. Rueda F, Schladow G. Dynamics of Large Polymictic Lake. II: Numerical Simulations. *Journal of Hydraulic Engineering* 2003; **129**: 92-101. DOI:10.1061/(ASCE)0733-9429(2003)129:2(92).

16. Schwab DJ, Beletsky D, DePinto J, Dolan DM. A hydrodynamic approach to modeling phosphorus distribution in Lake Erie. *Journal of Great Lakes Research* 2009; **35**: 50-60. DOI:http://dx.doi.org/10.1016/j.jglr.2008.09.003.

17. Smith PE. *A semi-implicit, three-dimensional model of estuarine circulation.* the United States Geological Survey (USGS): Sacramento, California, 2006.

18. Sullivan P, McWilliams J, Moeng C. A grid nesting method for large-eddy simulation of planetary boundary-layer flows. *Boundary-Layer Meteorology* 1996; **80**: 167-202. DOI:10.1007/BF00119016.

19. Taylor AH. Identifying forest reference conditions on early cut-over lands, lake Tahoe basin, USA. *Ecological Applications* 2004; **14**: 1903-1920. DOI:10.1890/02-5257.

20. Zavatarelli M, Pinardi N. The Adriatic Sea modelling system: a nested approach. *Annales Geophysicae* 2003; **21**: 345-364. DOI:10.5194/angeo-21-345-2003.

21. Zhai L, Sheng J, Greatbatch RJ. Application of a nested-grid ocean circulation model to Lunenburg Bay of Nova Scotia: Verification against observations. *Journal of Geophysical Research: Oceans* 2008; **113**: - C02024. DOI:10.1029/2007JC004230.

22. Zhang W, Hong H, Shang S, Chen D, Chai F. A two-way nested coupled tide-surge model for the Taiwan Strait. *Continental Shelf Research* 2007; **27**: 1548-1567. DOI:10.1016/j.csr.2007.01.018.